CLUMPY LANGMUIR WAVES IN TYPE III RADIO SOURCES: COMPARISON OF STOCHASTIC-GROWTH THEORY WITH OBSERVATIONS

P. A. ROBINSON
Department of Theoretical Physics and Research Center for Theoretical Astrophysics, School of Physics,
University of Sydney, NSW 2006, Australia

AND

I. H. CAIRNS AND D. A. GURNETT
Department of Physics and Astronomy, University of Iowa, Iowa City, IA 52242
Received 1992 June 18; accepted 1992 October 23

ABSTRACT

Detailed comparisons are made between the Langmuir-wave properties predicted by the recently developed stochastic-growth theory of type III sources and those observed by the plasma wave experiment on *ISEE 3*, after correcting for the main instrumental and selection effects. Analysis of the observed field-strength distribution confirms the theoretically predicted form and implies that wave growth fluctuates both spatially and temporally in sign and magnitude, leading to an extremely clumpy distribution of fields. A cutoff in the field-strength distribution is seen at a few mV m^{-1}, corresponding to saturation via nonlinear effects. Analysis of the size distribution of Langmuir clumps yields results in accord with those obtained in earlier work and with the size distribution of ambient density fluctuations in the solar wind. This confirms that the inhomogeneities in the Langmuir growth rate are determined by the density fluctuations and that these fluctuations persist during type III events.

Subject headings: plasma — solar wind — Sun: radio radiation

1. INTRODUCTION

This paper is concerned with making detailed comparisons between the Langmuir-wave properties predicted by the recently developed stochastic-growth theory of type III source regions (Robinson 1992b; Robinson, Cairns, & Gurnett 1992) and those observed in situ by the joint TRW-JPL-Iowa Plasma Wave experiment on *ISEE 3* (Scarf et al. 1978).

In the standard model of type III bursts (e.g., Ginzburg & Zheleznyakov 1958; Melrose 1990; Muschietti 1990; Robinson 1992b) Langmuir waves are generated via a beam instability of electrons streaming outward from the Sun. Most waves generated at the head of the beam are absorbed by electrons further back, thereby reducing the net energy loss to a level compatible with the observed propagation of beams to 1 AU or more from the Sun. When waves exceed the thresholds for three-wave decay and coalescence, secondary Langmuir and ion sound waves are generated, giving rise to radiation at the fundamental and second harmonic of the local plasma frequency. Inhomogeneous quasi-linear simulations (e.g., Grognard 1985) indicate that the beam propagates in a state close to marginal stability, in which wave growth just balances net losses. Such simulations also reproduce the approximate form of the electron distributions observed at 1 AU (Grognard 1985).

The standard model suffers from two shortcomings. First, observations have shown that ambient low-frequency density fluctuations in the solar wind have a level sufficient to scatter Langmuir waves out of resonance with the beam faster than they can grow (Celnikier et al. 1983; Celnikier, Muschietti, & Goldman 1987; Muschietti, Goldman, & Newman 1985). Second, the model does not explain the extreme clumpiness of the Langmuir waves, which show structure down to the shortest scales resolved (Gurnett & Anderson 1976, 1977; Lin et al. 1981, 1986) and vary by several orders of magnitude in energy density over periods of a second or less. A number of theories

have been proposed to circumvent one or other of these problems, based on nonlinear instabilities (e.g., Lin et al. 1986, and the references cited therein), local suppression or alignment of density fluctuations (Muschietti et al. 1985; Melrose, Dulk, & Cairns 1986; Melrose & Goldman 1987), or fluctuation-dependent growth rates and growth lengths (Smith & Sime 1979). Robinson (1992b) incorporated some of these ideas into a new model in which the beam propagates in a state close to marginal stability, but both beam and waves are perturbed by ambient density fluctuations. This leads to stochastic growth in which the growth rate fluctuates between positive and negative values and the logarithmic wave density undergoes a random walk, with positive net growth in localized regions.

Robinson (1992b) showed that the stochastic growth model can account for the presence of Langmuir waves, despite the mean growth rate being negative, and (semiquantitatively in his work) for the clumpiness and field-strength distribution of the waves. More recently, Robinson et al. (1992) showed that the stochastic-growth model implies that the Langmuir clump-size distribution should be the same as that of the ambient density fluctuations and confirmed this prediction by spectral analysis of *ISEE 3* wave-field data. It was also shown that several relationships between the variations of type III source parameters with distance from the Sun, predicted in part on the basis of stochastic-growth theory, are consistent with those actually observed (Robinson 1992a).

Given the initial successes of the stochastic-growth theory in accounting for the properties of type III sources, it is of considerable interest to test its predictions further. Data from the *ISEE 3* spacecraft have been used to study the predicted clumping of the Langmuir waves (Robinson et al. 1992). These data can also be compared with the predicted distribution of field strengths. Such an analysis not only enables the stochastic-growth theory to be tested, but allows us to add to

790

the existing knowledge of bursts which have been studied from other perspectives.

In § 2 we briefly review Robinson's (1992b) stochastic-growth model of Langmuir waves in type III source regions and generalize it to incorporate the existence of a nonlinear saturation level. In § 3 we outline the *ISEE 3* plasma wave observations that are considered here, discuss our choice of the specific type III events for analysis, and analyze the main instrumental effects on the data. Detailed comparisons between theory and observation are then made in § 4, focusing on the distributions of field strengths and spatial scales.

2. STOCHASTIC GROWTH OF LANGMUIR WAVES

In this section we briefly review Robinson's (1992b) stochastic growth model and discuss its generalization to incorporate both long-wavelength ambient density fluctuations with a spectrum of length scales (Robinson et al. 1992) and saturation of the growth via nonlinear interactions involving the beam driven waves (e.g., three-wave decay).

Ambient density fluctuations have been inferred to scatter Langmuir waves out of resonance with the beam at a typical rate of $\gtrsim (1-10)$ s^{-1}, whereas the largest growth rates for the observed electron beams (time averaged over 64 s) are $\lesssim (0.1-1)$ s^{-1} (Muschietti et al. 1985; Melrose et al. 1986; Robinson 1992b). Hence, under most if not all circumstances the waves cannot grow uniformly in space. Robinson (1992b) showed that the observed time-averaged growth rates are consistent with peak growth rates of a few times 10 s^{-1} in localized clumps of ~ 100 km in size. Hence, at least in regions where the scattering is not too large (e.g., where the gradient of the plasma density is approximately parallel to the beam direction), the beam-driven growth can overcome refraction of waves out of the growth region in wave vector space.

In the stochastic-growth model, the beam propagates in a state close to marginal stability, as implied by quasilinear calculations (which are unaffected *on average* by clumping; Melrose & Cramer 1989). Density fluctuations perturb the waves, allowing them to grow effectively only in localized clumps, while clumps of waves corresponding to unfavorable density fluctuations are damped. This in turn leads to perturbations of the beam (corresponding to spatial inhomogeneities in the beam distribution function) about its average state of marginal stability on time scales determined by the rate of change of the density fluctuations (see below). The growth rate thus fluctuates, while the space- and time-averaged effective growth rate is zero at marginal stability. Under these conditions waves in a given clump (defined to be simply a region of space of characteristic scale size of order that of the density fluctuations) C undergo a random walk in the logarithm of their energy density until either they leave the clump or wave growth saturates via nonlinear processes; this gives a characteristic interaction time $t_g \approx l/v_g$, where v_g is the group velocity of the Langmuir waves and l is the clump size. (In terms of the electron speed V and the beam speed v_b one has $v_g = 3V^2/v_b$.) During a time t_g, electrons traveling at velocity v_b reach the clump C from distances up to $v_b t_g$ away and traverse $\sim v_b t_g/l\langle l \rangle$ clumps in transit, where $\langle l \rangle$ is the mean clump size. Assuming these clumps have a characteristic lifetime $t_S \approx \langle l \rangle/v_S$, where v_S is the ion-sound speed, a typical upstream clump forms and disperses $\sim \langle t_g \rangle/t_S$ times near a particular location during the time t_g. Each upstream clump formation and dispersal "injects" a corresponding inhomogeneity into the part of the beam that interacts with the given clump C

during t_g. Hence, a total number $n_g(l)$ of beam inhomogeneities cross C during t_g, with

$$n_g(l) \approx \frac{v_b t_g}{\langle l \rangle} \frac{\langle t_g \rangle}{t_S} = \frac{v_b v_S l}{v_g^2 \langle l \rangle} . \tag{1}$$

A time $t \le t_g$ into the evolution of the clump, a typical number $n(t)$ of inhomogeneities will have passed by, with

$$n(t) = \frac{n_g t}{t_g} = \frac{t}{t_i} , \tag{2}$$

$$t_i = \frac{\langle l \rangle v_g}{v_b v_S} . \tag{3}$$

These estimates improve those of Robinson (1992b) and imply $n_g(\langle l \rangle) \gg 1$ for typical parameters from Table 1, with $v_S \approx (1 + 3T_i/T_e)^{1/2}(m_e/m_i)^{1/2} V$ in terms of the electron and ion temperatures and masses.

The total number of *e*-foldings G undergone by a clump of waves is the sum over individual increments $\Delta G \approx \Gamma t_i$ as the waves are encountered by each inhomogeneity in the beam, where the net growth rate Γ varies between inhomogeneities. The mean and variance of G are thus related to the corresponding quantities for ΔG by

$$\langle G \rangle = \langle \Delta G \rangle n(t) = \langle \Gamma \rangle t , \tag{4}$$

$$\sigma^2(G) = \sigma^2(\Delta G)n(t) = \sigma^2(\Gamma)t_i t , \tag{5}$$

for $t \le t_g$. Typical values are obtained by setting $t = t_g$ and $n_g = n_g(\langle l \rangle)$ in equations (4) and (5), which gives

$$\langle G \rangle = \langle \Delta G \rangle n_g = \frac{\langle \Gamma(l) \rangle l}{v_g} , \tag{6}$$

$$\sigma^2(G) = \sigma^2(\Delta G)n_g = \frac{\sigma^2[\Gamma(l)]l^2}{v_b v_g} . \tag{7}$$

Robinson et al. (1992) result $\Gamma(l) \sim l^{-1}$ has been used in obtaining the rightmost members of equations (6) and (7).

In terms of $\langle G \rangle$ and $\sigma \langle G \rangle$ the spatially averaged probability distribution of G is approximately

$$P(G) = \frac{1}{\sigma(G)(2\pi)^{1/2}} \exp \left[-\frac{(G - \langle G \rangle)^2}{2\sigma^2(G)} \right] , \tag{8}$$

via the Central Limit Theorem. The mean energy density in the waves is obtained by averaging $W \sim e^G$ over the distribution (8), using equations (4) and (5). This gives

$$\langle W \rangle = \exp \left\{ [\langle \Gamma \rangle + \tfrac{1}{2}\sigma^2(\Gamma)t_i]t \right\} , \tag{9}$$

for $t \le t_g$ (Robinson 1992b). Hence, the *effective* growth rate is

$$\Gamma_{\mathrm{eff}} = \langle \Gamma \rangle + \tfrac{1}{2}\sigma^2(\Gamma)t_i . \tag{10}$$

This result resolves the paradox of wave growth being observed in the presence of a negative *mean* growth rate $\langle \Gamma \rangle$ (Robinson 1992b) because Γ_{eff} can be positive even for $\langle \Gamma \rangle < 0$. The distribution $P(E)$ of electric field strengths E is obtained from equation (8) by writing $G = 2\ln(E/E_0)$, where E_0 is the characteristic initial field; this gives

$$E \, P(E) = P\left[\ln\left(\frac{E}{E_0} \right) \right]$$

$$= \frac{1}{\sigma(G)(2\pi)^{1/2}} \exp \left\{ -\frac{[2\ln(E/E_0) - \langle G \rangle]^2}{2\sigma^2(G)} \right\} . \tag{11}$$

TABLE 1
PARAMETERS OF 1979 FEBRUARY 8, FEBRUARY 17, AND MARCH 11 EVENTS

Quantity	Feb 8	Feb 17	Mar 11	Unit
N_e	7×10^6	1.2×10^7	2×10^6	m^{-3}
v_b	3.5×10^7	5×10^7	3.5×10^7	$m\ s^{-1}$
T_i	6×10^4	2.1×10^4	4×10^4	K
T_e	1.7×10^5	1.5×10^5	2×10^5	K
V	1.6×10^6	1.5×10^6	1.7×10^6	$m\ s^{-1}$
v_S	5.3×10^4	4×10^4	5.1×10^4	$m\ s^{-1}$
v_g	2.2×10^5	1.4×10^5	2.6×10^5	$m\ s^{-1}$
ω_p	1.5×10^5	2.0×10^5	8.2×10^4	s^{-1}
v_{sw}	3.5×10^5	3.5×10^5	4.8×10^5	$m\ s^{-1}$
$\Delta v_b/v_b$	0.1–0.2	0.3	0.1–0.2	...
$E_{A\ max}$	2.5×10^{-3}	4.0×10^{-3}	5.0×10^{-3}	$V\ m^{-1}$
E_{max}	2.7×10^{-3}	4.8×10^{-3}	5.3×10^{-3}	$V\ m^{-1}$
n_g	38	100	26	...
t_g	0.4	0.6	0.3	s
t_i	0.011	0.006	0.013	s
$\sigma(G)$	4.2	2.8	4.5	...
$\sigma(\Delta G)$	0.7	0.3	0.9	...
$\sigma[\Gamma(l)]$	57	37	68	s^{-1}
$\langle G \rangle$	-8.8	-3.8	-10	...
$\langle \Delta G \rangle$	-0.2	-0.04	-0.4	...
$\langle \Gamma(l) \rangle$	-10	-3	-13	s^{-1}
E_{Ac}	3×10^{-3}	4×10^{-3}	6×10^{-3}	$V\ m^{-1}$
E_c	3×10^{-3}	5×10^{-3}	$\gtrsim 7 \times 10^{-3}$	$V\ m^{-1}$
E_{Apk}	1.3×10^{-5}	1.3×10^{-4}	8.5×10^{-6}	$V\ m^{-1}$
E_{pk}	3.5×10^{-5}	2.8×10^{-4}	2.4×10^{-5}	$V\ m^{-1}$
a	1.7	1.5	1.75	...
b	2.3	3.0	2.5	...
ω_0	0.4	0.8	0.6	s^{-1}

NOTES.—Most parameters are from Lin et al.'s (1981, 1986) papers, or from the National Space Science Data Center's OMNI database. No estimate of T_e for the 1979 February 17 event was available, so we have used a typical value of 1 AU. Note that $l = 200$ km is assumed in the evaluation of $\langle \Gamma(l) \rangle$ and $\langle \sigma[\Gamma(l)] \rangle$, and $\langle l \rangle = 90$ km is assumed in evaluating t_g and t_i.

The stochastic growth theory therefore predicts a parabolic shape for $\ln[E\ P(E)]$ when plotted as a function of $\ln E$. In § 4 we show that this theoretical prediction is consistent with the observational data. (Note that the form of the distribution [11] is valid only for fields above the thermal level. This implies that the normalization should be adjusted accordingly. However, the thermal level, estimated below, turns out to be far below the observed fields, implying that this is a relatively small correction. Since, in addition, the absolute normalization is not investigated in the present work, we do not make this refinement here.)

Stochastic growth leads to arbitrarily high wave levels in a vanishingly small proportion of clumps, a situation that is prevented by the existence of a nonlinear saturation mechanism. If the highest wave levels saturate via three-wave decay (or, more generally, via some other nonlinear process [see, e.g., Cairns 1984, 1986; Lin et al. 1986; Robinson, Willes, & Cairns 1993]), the distribution of G will fall off rapidly beyond the point G_c corresponding to the threshold field E_c for decay. Dynamically, the energy density of those waves that exceed the threshold decreases suddenly as product waves are generated, falling to an asymptotic level that is an exponentially decreasing function of the extent to which the threshold was exceeded (Robinson 1992c). In order to calculate $P(G)$ near the three-wave threshold we approximate the threshold as an absorbing boundary (Robinson 1992c) and solve the diffusion problem in G for the half-interval $G < G_c$. This is most easily done by the method of images in which a symmetrically placed distribution of opposite sign, centered at $2G_c - \langle G \rangle$, diffuses in the half-

interval $G_c < G$. After normalizing the unit total probability the result is

$$P(G) = \left[\sigma(G)(2\pi)^{1/2} \ \mathrm{erf}\left(\frac{G_c - \langle G \rangle}{\sigma(G)\sqrt{2}} \right) \right]^{-1}$$
$$\times \left\{ \exp\left[-\frac{(G - \langle G \rangle)^2}{2\sigma^2(G)} \right] \right.$$
$$\left. - \exp\left[-\frac{(2G_c - \langle G \rangle - G)^2}{2\sigma^2(G)} \right] \right\}, \quad (12)$$

for $G < G_c$, and $P(G) = 0$ for $G > G_c$. Figure 1 shows the distributions (8) and (12) and illustrates the effect of the decay threshold. The electric-field distribution is obtained from distribution (12) by using $G = 2\ln(E/E_0)$, as before.

Robinson et al. (1992) found that values of G can be described as being spatially distributed in clumps of width l and (without loss of generality) unit height. The probability distribution $P_G(l)$ of the clump size was found to have the approximate form

$$P_G(l) \sim \begin{cases} l^{-a}, & l_0 < l < l_{max}, \\ l^{-b}, & l_{min} < l < l_0, \end{cases} \quad (13)$$

which gives the mean values

$$\langle l \rangle \approx \frac{b-1}{b-2} l_{min}, \quad (14)$$

$$\langle l^2 \rangle \approx \frac{b-1}{3-a} l_{min}^{b-1} l_0^{a-b} l_{max}^{3-a}, \quad (15)$$

where some small terms have been neglected for the case relevant to the solar wind, which has $a \approx 1.5$ and $b \approx 2.5$ (Robinson et al. 1992). In the solar wind l_{min} is the smallest fluctuation size consistent with observation (Celnikier et al. 1983, 1987) and with moderate to weak dissipation of Langmuir waves. These constraints give $0.4\ \mathrm{km} \lesssim l_{min} \lesssim 30\ \mathrm{km}$ in general and $2\ \mathrm{km} \lesssim l_{min} \lesssim 30\ \mathrm{km}$ for beam-driven waves, for which l_{min} must also exceed the wavelength $2\pi v_b/\omega_p$ (Robinson et al. 1992). The maximum scale l_{max} is determined by the
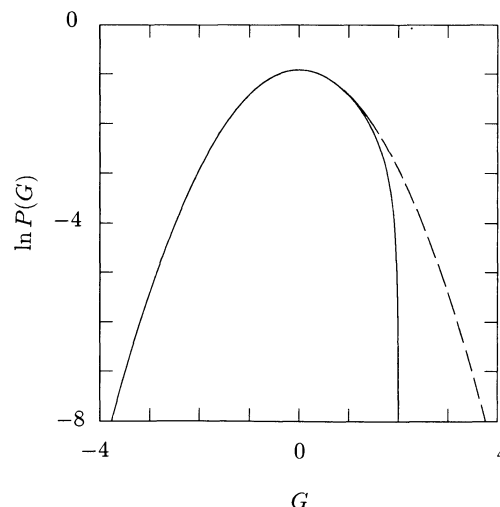

FIG. 1.—Theoretical distribution $P(G)$ with and without the presence of a three-wave decay threshold as given by eqs. (8) and (12) (*solid and dashed curves, respectively*).

distance that the Langmuir waves can remain in resonance with the marginally stable beam, giving

$$l_{max} \approx \frac{3rV^2 \Delta v_b}{2v_b^3} , \qquad (16)$$

where r is the distance from the Sun and Δv_b the spread in beam velocities (Melrose et al. 1986; Robinson et al. 1992). Using $l_{max} = 5 \times 10^4$ km, $l_0 \approx 4 \times 10^3$ km, and $l_{min} = 30$ km for $a = 1.5$ and $b = 2.5$, we find

$$\langle l \rangle \approx 90 \text{ km} , \qquad (17a)$$

$$\langle l^2 \rangle \approx (700)^2 \text{ km}^2 . \qquad (17b)$$

Robinson et al. (1992) found the result $G \propto n$, where n is the density fluctuation and, hence, predicted the distribution $P_n(l)$ of ambient density fluctuations to satisfy

$$P_n(l) = P_G(l) . \qquad (18)$$

This result was verified to within the observational uncertainties in their work.

The time t for which a clump is detected at a spacecraft is proportional to its width, with $t = l/v_{sw}$, where v_{sw} is the solar wind speed. The observed time history of G (or of log E) is the sum of contributions from individual clumps. If we assume these clumps are uncorrelated, the total power spectrum $S(\omega)$ is the integral, weighted by $P_G(t)$, over the spectra $S(\omega; t)$ of individual clumps of characteristic duration t. This gives (Robinson et al. 1992)

$$S(\omega) \propto \begin{cases} \omega^{a-3} , & \omega \ll \omega_0 , \\ \omega^{b-3} , & \omega_0 \ll \omega , \end{cases} \qquad (19)$$

with $\omega_0 t_0 = \omega l_0/v_{sw} \approx 1$; this result is independent of the shape of the clumps. The spectrum plateaus for $\omega \lesssim 1/t_{max}$ and depends on the shape of the clumps for $\omega \gtrsim 1/t_{min}$.

3. OBSERVATIONS AND INSTRUMENTAL EFFECTS

In this section we briefly discuss the choice of type III events analyzed in this work. Instrumental effects resulting from filter responses, antenna projection effects, and other sources are then discussed.

3.1. Data Selection

The data used in this work were obtained from the joint TRW-JPL-Iowa plasma wave instrument on *ISEE 3* (Scarf et al. 1978), which was located in the solar wind 1.6×10^6 km ($259R_E$) upstream of Earth where R_E is the radius of the Earth. The data consist of time series of electric field strengths measured over 0.5 s intervals and sampled simultaneously in each of 16 frequency channels. These channels cover the frequency range 17.8 Hz to 100 kHz, 4 per frequency decade. Each channel up to 5.6 kHz has a characteristic full bandwidth of 30%, while the bandwidths of the remainder are 15%.

Three type III events are considered below: (1) 1979 February 8 from 06:30 UT to 08:00 UT, (2) 1979 February 17 from 19:30 UT to 22:00 UT, and (3) 1979 March 11 from 11:00 to 12:00 UT. The reason for the choice of these particular events is that they have previously been studied in detail from other perspectives involving both particle and wave measurements (the first and third by Lin et al. 1986, and the second by Lin et al. 1981). Hence, the present study can both make use of an extend existing knowledge of these events.

3.2. Filter Rolloff Effects

In § 4 we are concerned with data from pairs of channels bracketing the plasma frequency during type III events, either the 10 kHz and 17.8 kHz channels, or the 17.8 kHz and 31.6 kHz channels. These channels respond both to Langmuir waves near the plasma frequency and to the electromagnetic waves that form the type III radio burst.

For narrow-band waves at a frequency f located between the central frequencies f_a and f_b of the channels immediately above and below f, respectively, the measured fields in the two channels are related to the true field E_A on the antenna by

$$E_a = E_A 10^{r(f/f_a)} , \qquad (20a)$$

$$E_b = E_A 10^{r(f/f_b)} , \qquad (20b)$$

where $r(\rho)$ is the filter response function. Thus, if E_a, E_b and r are known, f and E_A can be calculated. Figure 2 shows the measured form of $r(\rho)$ for filters used in the *ISEE 1*, *ISEE 2*, and CRRES plasma wave instruments (R. R. Anderson 1991, private communication); filters of the same design were used in the *ISEE 3* instrument (E. W. Greenstadt & R. R. Anderson 1991, private communications), but calibration data for the actual filters flow on *ISEE 3* are currently unavailable (E. Greenstadt 1991, private communication). The true field and frequency can be approximated by

$$E_A \approx 13(E_a E_b)^{1/2} , \qquad (21)$$

$$f/f_a \approx 1 - 0.043 \ln(180E_b/E_a) . \qquad (22)$$

Figures 3a and 3b show E_A/E_a and f/f_a, respectively, as functions of E_b/E_a. Solid curves are obtained numerically from the measured response function, while dashed curves are from the approximations (21) and (22).

3.3. Projection Effects

The field E_A detected by the *ISEE 3* antenna is the component of the true field E projected onto the antenna direction $\hat{a}$. Since the exact direction of E is unknown, it is not possible to correct individual data for this effect. However, it *is* possible to estimate the effect on the overall statistical distribution of fields and show that it can be neglected in the cases of interest to us. This is the approach we follow here.
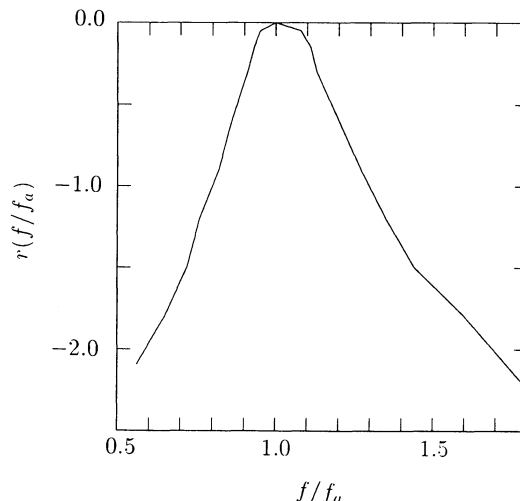

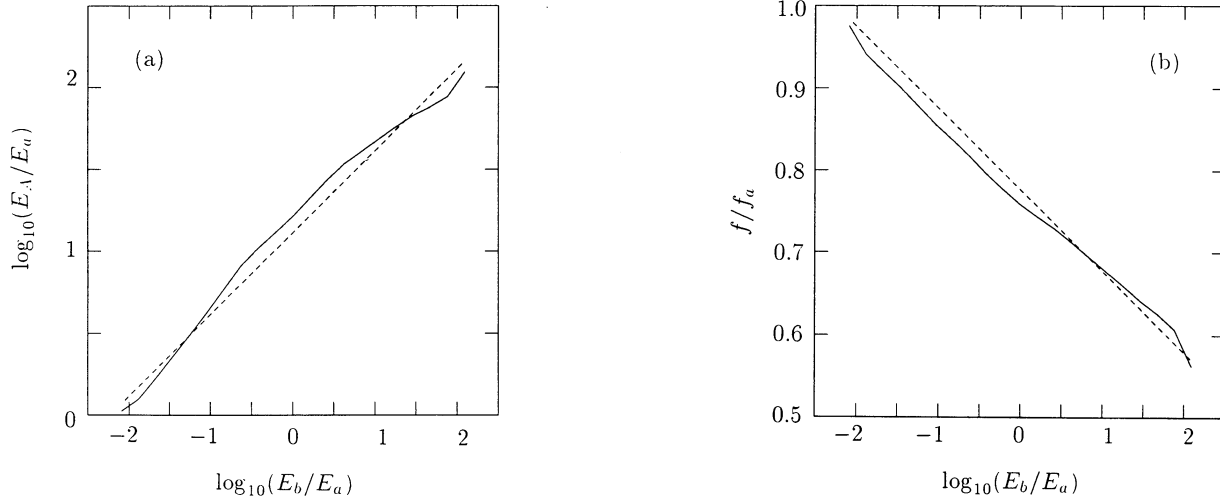FIG. 2.—Measured filter response (rolloff) function $r(\rho)$

FIG. 3.—Parameters corrected for rolloff effects. Solid curves show results using the measured response, while dashed curves show approximate results. (a) E_A/E_a vs. E_b/E_a, with the dashed curve from eq. (21). (b) f/f_a vs. E_b/E_a, with the dashed curve from eq. (22).

During its rotation (period ≈ 3 s) the antenna's angle θ_A relative to the interplanetary magnetic field $\boldsymbol{B}$ sweeps through almost the full range $0° \leq \theta_A \leq 360°$, because the field lies close to the (ecliptic) plane in which the antenna rotates. Since the strangest Langmuir fields lie approximately in the direction of $\boldsymbol{B}$, the measured field will underestimate the true ones by large factors when $|\cos \theta_A|$ is small. If we approximate the relative directions of $\boldsymbol{B}$ and $\hat{\boldsymbol{a}}$ as being distributed uniformly in θ_A between fixed values of azimuth relative to $\boldsymbol{B}$, the probability distribution $P_A(E_A)$ of E_A is determined by the distribution $P(E)$ of true fields having $E > E_A$. This gives

$$P_A(E_A) = \int_0^1 \frac{d\mu}{\mu} P\left(\frac{E_A}{\mu}\right) , \quad (23)$$

where $E_A = \mu E$.

The integral in equation (23) can be evaluated analytically for the predicted distribution (11) by making the change of variable $u = 2 \ln \mu$. This yields

$$E_A P(E_A) = \frac{1}{2} \exp\left[\frac{4x + \sigma^2(G)}{8}\right] \text{erfc}\left[\frac{2x + \sigma^2(G)}{2\sigma(G)\sqrt{2}}\right] , \quad (24)$$

$$\approx \frac{2\sigma^2(G)}{2x + \sigma^2(G)} \frac{1}{\sigma(G)(2\pi)^{1/2}} \exp\left[-\frac{x^2}{2\sigma^2(G)}\right] , \quad (25)$$

with

$$x = 2 \ln (E_A/E_0) - \langle G \rangle . \quad (26)$$

The approximation (25) is valid for

$$2x + \sigma^2(G) \gtrsim 2\sigma(G)\sqrt{2} , \quad (27)$$

a condition that is found to be satisfied by the data discussed in § 4 [$\sigma(G) \sim 4$, $x \gtrsim 0$]. Comparison of equation (25) with equation (11) shows that the two distributions are the same except for the factor $2\sigma^2(G)/[2x + \sigma^2(G)]$, which is of order unity for the parameters of interest in § 4. Thus $\sigma(G)$ will be essentially unaffected, a result that is valid even in the case in which there is no correlation between the antenna direction and $\boldsymbol{B}$. Similarly, the *number* of observations at high E will not be significantly reduced, because the change in normalization is of order unity. One effect that should be noted and corrected for when analyzing data is the offset of the peak toward the left as $\sigma(G)$

increases, as seen in Figure 4, which shows $E_A P(E_A)$ for $\sigma(G) = 0.5, 1, 2,$ and 4. The distribution $E P(E)$ for $\sigma(G) = 2$ is also shown (dashed) for comparison, demonstrating that the shape of the high-E distribution is unchanged by projection effects and that the approximation (25) is adequate where (27) is satisfied.

In a distribution like (24) that decreases steeply at large E, projection effects do not make much difference to the highest field E_{max} observed in a set of N observations. This field is determined by the condition that less than one even higher field is statistically likely to be observed in the N measurements, i.e. by

$$N \int_{E_{A\,max}}^{\infty} dE_A P(E_A) = 1 . \quad (28)$$

The exponentially rapid fall-off in $P(E)$ large E implies that the change of order unity in normalization between the high-E distributions (11) and (25) has only a slight effect on E_{max} (reducing it $E_{A\,max}$) because even a large fractional reduction in
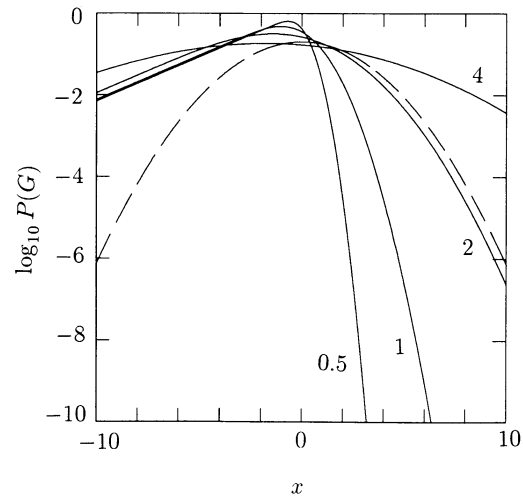

FIG. 4.—Projection effects on the distribution, showing $E_A P(E_A)$ vs. x (with $x = 2 \ln (E_A/E_0) - \langle G \rangle$) from eq. (24) for $\sigma(G) = 0.5, 1, 2,$ and 4, as labeled. The true distributions are Gaussians of the form (11) centered at $x = 0$, one of which is shown (*dashed curve*) for $\sigma(G) = 2$.

the probability of observing a very high field is compensated for by a slight decrease in the lower bound of the integral in (28) where $P(E_A)$ is relatively large. We can estimate this effect by noting

$$\int_{E_{A\,max}}^{\infty} dE_A\, P(E_A) = \int_{E_{max}}^{\infty} dE\, P(E) \,. \tag{29}$$

Upon substituting equations (11) and (25) and using the asymptotic form for the error functions that result from the integrals, equation (29) yields

$$\frac{E_{max}}{E_{A\,max}} \approx \left[\frac{\sigma^2(G) + 2x_{A\,max}}{2\sigma^2(G)}\right]^{\sigma^2(G)/(2x_{A\,max})} , \tag{30}$$

where $x_{A\,max}$ is the value of x corresponding to $E_{A\,max}$. The estimate (30) is verified for $\sigma(G) = 2$ by comparing the dashed curve in Figure 4 with the corresponding solid curve.

3.4. *Other Effects*

The automatic gain control (AGC) used for each of the 16 channels in the main *ISEE 3* filter bank has a rise time $\delta t \approx 10$ ms, a decay time of order 50 ms, and a mean settling time comparable to the sampling interval of 0.5 s. Clumpy fields with scales small compared with the distance the solar wind travels during the rise time (i.e., with $l \lesssim v_{sw}\,\delta t \approx 4$ km) will therefore be seriously underestimated. If a significant fraction

of fields have scales smaller than 4 km, this will result in an underestimation of the highest fields and a reduction in their apparent probability; however, this appears unlikely since the shortest scale length for beam-driven waves is at least 2 km, as discussed following equation (15). Moreover, since each AGC ideally settles during the 0.5 s sampling interval and the rise and decay times are much smaller than 0.5 s, the electric field and clump distributions derived here should be unaffected by AGC effects. Our analyses are, in any case, necessarily restricted to scales greater than the resolution limit of 200 km (i.e., $l/v_{sw} \sim 0.5$ s). Information on scales $\lesssim 200$ km must await analyses of data from the Ulysses, Galileo and ISTP missions.

4. COMPARISON WITH OBSERVATIONS

In this section we analyze the data from the 1979 February 8, February 17, and March 11 events and compare the results with the theoretical predictions from § 2. In particular, we are concerned with the statistical distributions of field strengths and Langmuir clump sizes.

4.1. *Field-Strength Statistics*

Before commencing detailed analysis of fields corrected for instrumental effects, we first consider the raw data from one event to provide a baseline against which to judge the effects of rolloff corrections. Figures 5a and 5b show the time series from the 17.8 and 31.6 kHz channels, respectively, for the 1979 Feb-
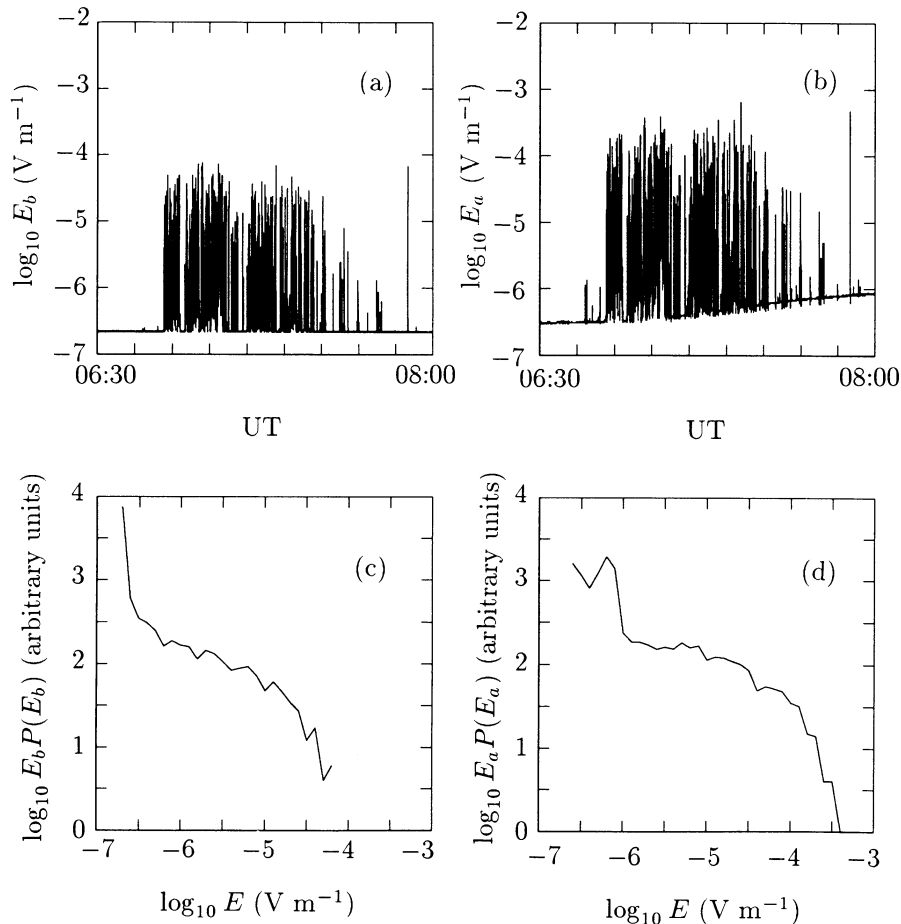

FIG. 5.—Raw data from the 1979 February 8 event. (*a*) E_b vs. *t* in the 17.8 kHz channel. (*b*) E_a vs. *t* in the 31.6 kHz channel. (*c*) $E_b P(E_b)$ for the 17.8 kHz channel. (*d*) $E_a P(E_a)$ for the 31.6 kHz channel.
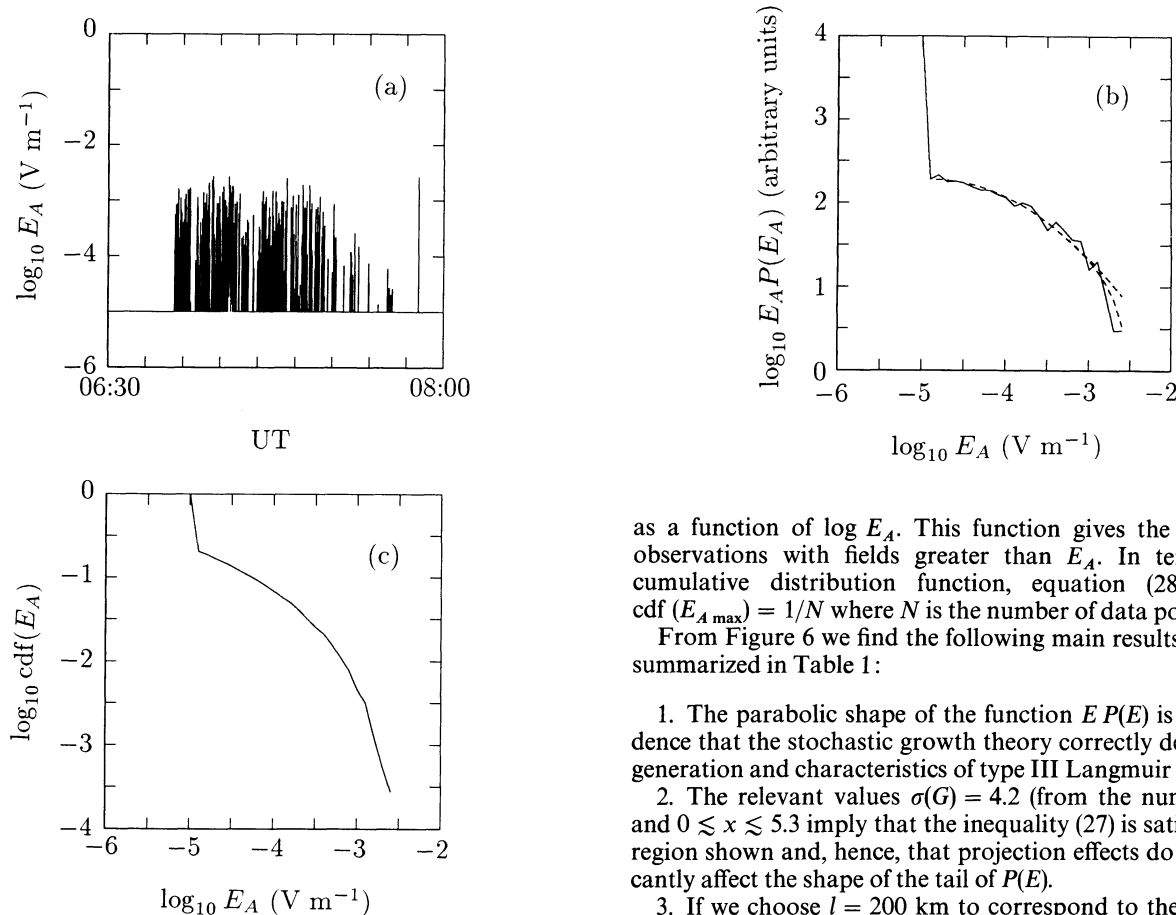
FIG. 6.—Data from the 1979 February 8 event, corrected for rolloff effects. (a) E_A vs. t. (b) $E_A P(E_A)$ (solid curve) and fits from eqs. (11) and (12) (upper and lower dashed curves, respectively). (c) Cumulative distribution function.

ruary 8 event. The characteristic highly impulsive nature of the Langmuir waves is visible in both channels, indicating that the plasma frequency f_p lies between them, in accord with the estimate $f_p \approx 24$ kHz obtained from the in situ density measurement (Lin et al. 1986). Smoothly rising electromagnetic emission is seen in the 31.6 kHz channel, beginning at approximately 06:55 UT. The probability distributions of raw electric field strengths $P(E)$ in the 17.8 and 31.6 kHz channels (E_b and E_a, respectively) are shown in Figures 5c and 5d, respectively, in the form $E P(E)$. Both plots show large peaks toward the left, corresponding to signals at or near the instrumental threshold and, in Figure 5d, to electromagnetic waves. The remainder of the curves, which show the statistics of Langmuir waves detected above both the threshold and the electromagnetic background, have the characteristic approximately parabolic shape expected from (11) and (25).

Correction of the data in Figures 5a and 5b for filter rolloff effects yields the time series of E_A shown in Figure 6a, where all fields below the bound imposed by the instrumental threshold and electromagnetic background have been omitted. Figure 6b shows the corresponding function $E_A P(E_A)$ together with least-squares fits to the theoretical expressions (11) and (12). Figure 6c shows the cumulative distribution function

$$\text{cdf } (E_A) = \int_{E_A}^{\infty} P(E')dE' , \qquad (31)$$

as a function of log E_A. This function gives the fraction of observations with fields greater than E_A. In terms of the cumulative distribution function, equation (28) becomes cdf $(E_{A\,\text{max}}) = 1/N$ where N is the number of data points.

From Figure 6 we find the following main results, which are summarized in Table 1:

1. The parabolic shape of the function $E P(E)$ is strong evidence that the stochastic growth theory correctly describes the generation and characteristics of type III Langmuir waves.

2. The relevant values $\sigma(G) = 4.2$ (from the numerical fits) and $0 \lesssim x \lesssim 5.3$ imply that the inequality (27) is satisfied in the region shown and, hence, that projection effects do not significantly affect the shape of the tail of $P(E)$.

3. If we choose $l = 200$ km to correspond to the resolution of the *ISEE 3* measurements and use the other parameters listed in Table 1, equations (6) and (7) imply $\sigma(\Delta G) \approx 0.7$ and $\sigma[\Gamma(l)] \approx 57$ s^{-1}. This value of $\sigma[\Gamma(l)]$ is consistent with the observed values of the mean slopes of type III beams, because the latter, averaged over 64 s, do not reflect the instantaneous values of Γ. Robinson (1992b) showed that the observed mean slopes are consistent with $\sigma[\Gamma(l)]$ of a few times 10 s^{-1} for $l \sim 100$ km, as found here.

4. If marginal stability is assumed on average ($\Gamma_{\text{eff}} = 0$), equation (10) implies $\langle G \rangle = -\sigma^2(G)/2 \approx -8.8$. Using equation (6) we find $\langle \Gamma(l) \rangle \approx -10$ s^{-1}, and $\langle \Delta G \rangle \approx -0.2$ for the same parameters as in point 2, above. Since $\sigma[\Gamma(l)] \approx 57$ s^{-1} from point (3) above, we find $\sigma[\Gamma(l)] \gg |\langle \Gamma(l) \rangle|$, which implies that there is instantaneous growth of Langmuir waves in nearly half the plasma. (Note that the value $\sigma[\Gamma(l)]/\langle \Gamma(l) \rangle = -2(v_b/v_g)^{1/2}/\sigma(G) \approx -6$ is independent of l.) However, clumps in which net growth is positive for more than a few t_i are rare, consistent with the highly inhomogeneous qualitative nature of the observed waves. The waves in a given clump typically grow or damp by less than one e-folding for each beam inhomogeneity that passes by. For $\sigma[\Gamma(l)] = 57$ s^{-1} and $\langle \Gamma(l) \rangle = -10$ s^{-1}, the maximum instantaneous growth rate is ~ 100 s^{-1}, consistent with Robinson (1992b) and Melrose & Goldman (1987).

5. The characteristic measured field strength is the field at the peak of the distribution, E_{pk}. The numerical fit gives $E_{A\text{pk}} \approx 13$ μV m^{-1}. After correction for the offset illustrated in Figure 4 with $\sigma(G) = 4.2$, the corresponding true field is $E_{\text{pk}} \approx 35$ μV m^{-1}.
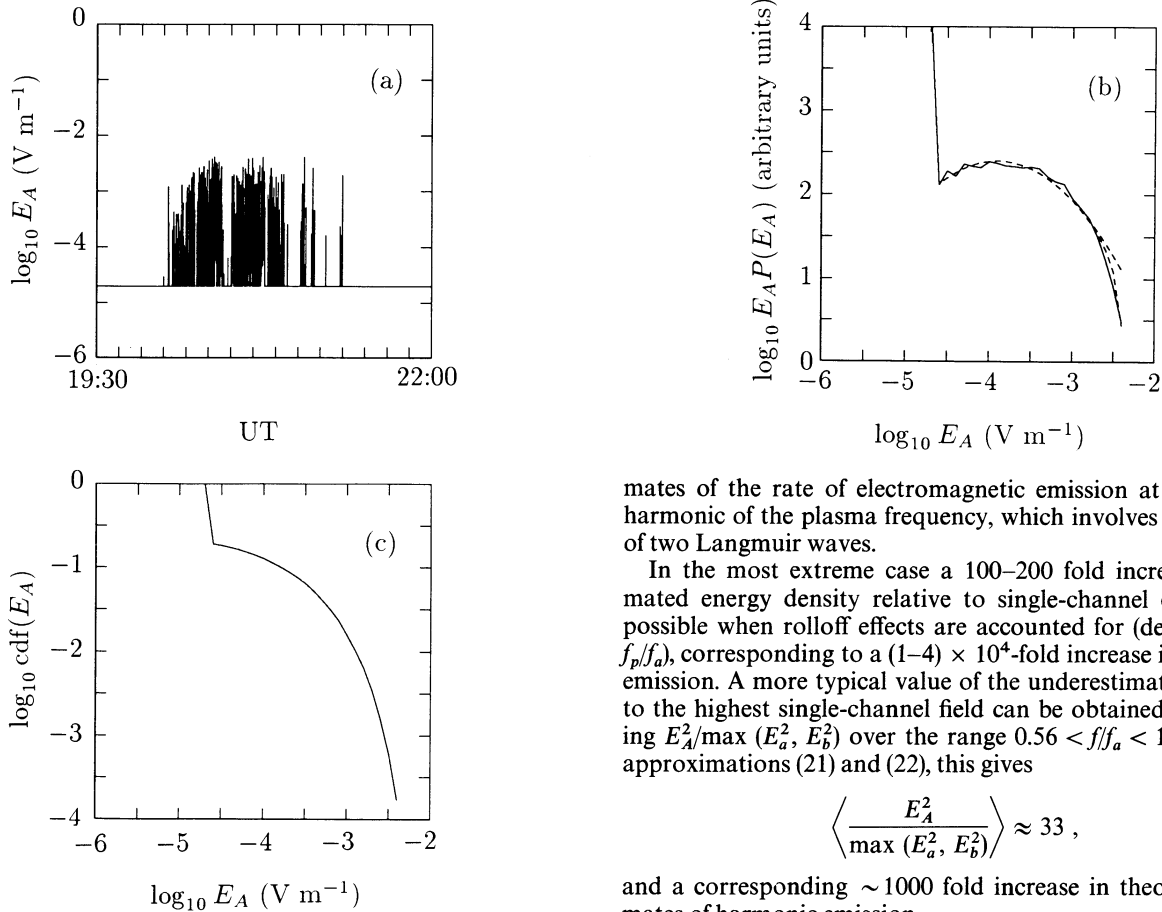
For comparison, the thermal level of Langmuir waves with

FIG. 7.—Data from the 1979 February 17 event, corrected for rolloff effects. (a) E_A vs. t. (b) $E_A P(E_A)$ (*solid curve*) and fits derived from eqs. (11) and (12) that neglect and include the nonlinear cutoff E_c (*upper and lower dashed curves, respectively*). (c) Cumulative distribution function.

$k \lesssim 0.2k_D$ (the point at which strong damping cuts in, even in the absence of a nonthermal tail) can be estimated from

$$\epsilon_0 E_{Th}^2 \approx k_B T_e \left(\frac{0.2k_D}{2\pi}\right)^3 , \qquad (32)$$

where E_{Th} is the rms thermal field strength. Equation (32) gives $E_{Th} \approx 0.08 \ \mu\text{V m}^{-1}$, which is much less than E_{pk}. This is in accord with our picture of type III events in which the head of the unstable electron beam drives Langmuir waves to high levels before attaining marginal stability in a very short period, after which the waves evolve according to stochastic-growth theory, with negative mean growth.

6. The highest field seen was $E_{A\,max} \approx 2.5 \ \text{mV m}^{-1}$, ~ 4 times higher than the highest detection in a single channel (see Fig. 5 and Lin et al. 1986). Equation (30) then gives $E_{max} \approx 2.7 \ \text{mV m}^{-1}$. Effects such as the finite AGC rise times, mentioned in § 2 but not considered here, could raise E_{max} further if intense wave packets with $l \lesssim 4$ km are present. However, detection of such packets with the *ISEE 3* instrument is unlikely owing to both their small size and the relative infrequency of the highest field strengths.

The value of E_{max} found here is ~ 4 times higher than that estimated from either channel alone. This gives an order of magnitude higher energy density than previously recognized to drive potential nonlinear processes such as three-wave decay and wave collapse and will cause a ~ 250 fold increase in esti-

mates of the rate of electromagnetic emission at the second harmonic of the plasma frequency, which involves coalescence of two Langmuir waves.

In the most extreme case a 100–200 fold increase in estimated energy density relative to single-channel estimates is possible when rolloff effects are accounted for (depending on f_p/f_a), corresponding to a $(1–4) \times 10^4$-fold increase in harmonic emission. A more typical value of the underestimation relative to the highest single-channel field can be obtained by averaging $E_A^2/\text{max} \ (E_a^2, E_b^2)$ over the range $0.56 < f/f_a < 1$. Using the approximations (21) and (22), this gives

$$\left\langle \frac{E_A^2}{\text{max} \ (E_a^2, E_b^2)} \right\rangle \approx 33 , \qquad (33)$$

and a corresponding ~ 1000 fold increase in theoretical estimates of harmonic emission.

7. The probability distribution falls more rapidly at high E than the fit made using equation (11), which does not allow for the presence of a cutoff due to nonlinear processes. A better fit is obtained using equation (12) with $E_{Ac} = 3 \ \text{mV m}^{-1}$, as shown by the lower dashed curve in Figure 6b. We note that this faster-than-Gaussian fall-off in $P(E)$ strengthens the statistical case for $E_{A\,max} \approx E_{max}$, since there are even fewer high fields available to be projected down to $E_A = 2.5 \ \text{mV m}^{-1}$. We find $E_c \approx 3.3 \ \text{mV m}^{-1}$ from equation (30).

The nonlinear process that appears most likely to determine E_c is three-wave decay of Langmuir waves into product Langmuir and ion-sound waves. The strongest pieces of evidence in favor of this mechanism are, first, the observation of burst of ion-sound waves at approximately the correct frequency simultaneously with the strongest bursts of Langmuir waves (Cairns 1984; Lin et al. 1986), and second, the close correlation between the amplitudes of the two waves (Lin et al. 1986; Muschietti 1990). We consider this process and its competitors (e.g., nonlinear wave collapse) in detail in a later paper in which stochastic-growth theory is extended to incorporate nonlinear processes (Robinson et al. 1993).

8. The cumulative distribution function shown in Figure 6c has a sharp step at the threshold field implied by instrumental limits and electromagnetic emission, reflecting the large number of fields below this level. Above this point $\log_{10} [\text{cdf} \ (E_A)]$ is approximately parabolic when plotted against $\log_{10} E_A$, as would be expected from integration of the asymptotic form (25).

Figures 7a and 8a show the time series of E_A for the 1979 February 17 and March 11 events, respectively, while Figures
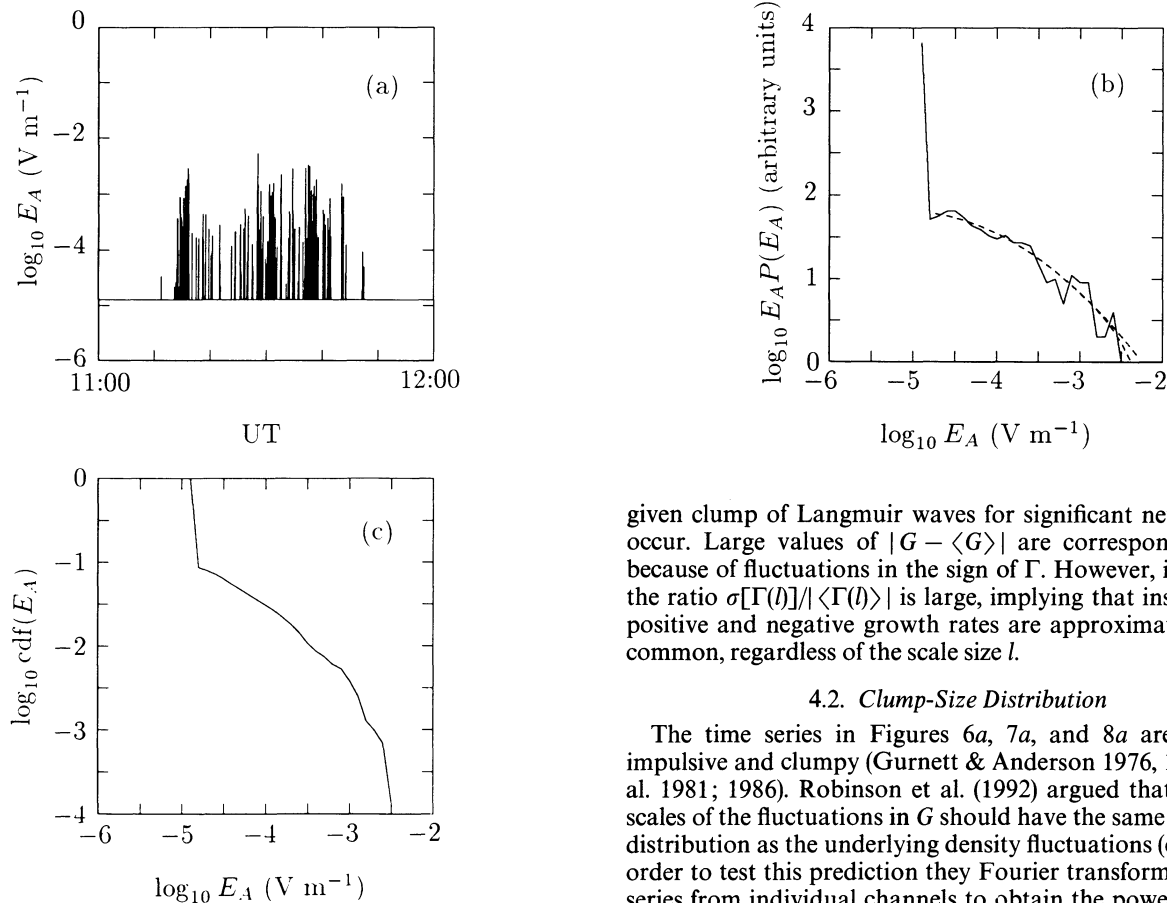
FIG. 8.—Data from the 1979 March 11 event, corrected for rolloff effects. (a) E_A vs. t. (b) $E_A P(E_A)$ (solid curve) and fits from eqs. (11) and (12) (upper and lower dashed curves, respectively). (c) Cumulative distribution function.

7b and 8b show the corresponding probability distributions, and Figures 7c and 8c show the cumulative distribution functions. The parameters obtained from fitting this data with the theoretical expressions are given in Table 1. In most respects the results for the three events in Figures 6–8 are similar. Several points worth noting are:

1. The peak of the parabolic distribution in Figure 7b lies well clear of the lower bound imposed by the instrumental threshold and electromagnetic background. This confirms the predicted parabolic form of the statistical distribution more strongly than the results in Figure 6, but the cutoff is too high to reveal the relatively flat behavior seen at small E_A in Figure 4.

2. The values of $E_{A\,max}$ and E_{Ac} are similar for all three events, at a few mV m^{-1}, despite E_{Apk} being a factor of 10 higher in Figure 7b. This implies that the saturation mechanism cuts in at a characteristic level, independent of the strength with which the Langmuir waves are driven. The consequences of this are investigated in detail elsewhere (Robinson et al. 1993). Figure 7b shows the effects of the nonlinear cutoff most clearly with a ∼5 fold difference between the simple parabolic fit (11) and the actual distribution at $E_{A\,max}$. The cutoff field is not well determined from Figure 8b and may be somewhat higher than our estimate of 7 mV m^{-1}.

3. The results in Figures 7 and 8 confirm $|\langle \Delta G \rangle| < 1$ and imply that many beam inhomogeneities must interact with a

given clump of Langmuir waves for significant net growth to occur. Large values of $|G - \langle G \rangle|$ are correspondingly rare because of fluctuations in the sign of Γ. However, in each case the ratio $\sigma[\Gamma(l)]/|\langle\Gamma(l)\rangle|$ is large, implying that instantaneous positive and negative growth rates are approximately equally common, regardless of the scale size l.

4.2. Clump-Size Distribution

The time series in Figures 6a, 7a, and 8a are extremely impulsive and clumpy (Gurnett & Anderson 1976, 1977; Lin et al. 1981; 1986). Robinson et al. (1992) argued that the length scales of the fluctuations in G should have the same probability distribution as the underlying density fluctuations (eq. [18]). In order to test this prediction they Fourier transformed the time series from individual channels to obtain the power spectra of G, using a Monte Carlo method to remove instrumental effects. Their method is

1. Construct a Monte Carlo distribution of the form (13) using rectangular clumps of unit height.
2. Calculate the mean and standard deviation of the Monte Carlo distribution.
3. If the observational cutoff occurs a certain number of standard deviations from the observational mean of log E, cut off the Monte Carlo distribution at the same point in terms of its own mean and standard deviation. (N.B. This step must be iterated until it converges, with the mean and standard deviation being those of the cutoff distribution itself.)
4. Fourier transform both the observational and (cutoff) Monte Carlo time series and adjust the Monte Carlo parameters a, b, and ω_0 until the two spectra match when equivalently normalized. Uncertainties in the parameters of the best fit can be determined at this point.
5. Determine the true underlying spectrum by Fourier transforming the original Monte Carlo time series (without instrumental cutoffs) for the best-fit cases.

Here we carry out this procedure for time series that have been corrected for rolloff effects in order to obtain improved estimates of the parameters a, b, and ω_0 in equation (19).

Figures 9a–9c show the raw spectra and corresponding Monte Carlo fits for the 1979 February 8, February 17, and March 11 events. The parameters of the fits, listed in Table 1, are consistent with those found by Robinson et al. (1992), with $a = 1.5$–1.75, $b = 2.3$–3.0, and $\omega_0 = 0.4$–0.8 (with uncertainties of ± 0.1 in a and b and ± 0.2 s^{-1} in ω_0). The corresponding
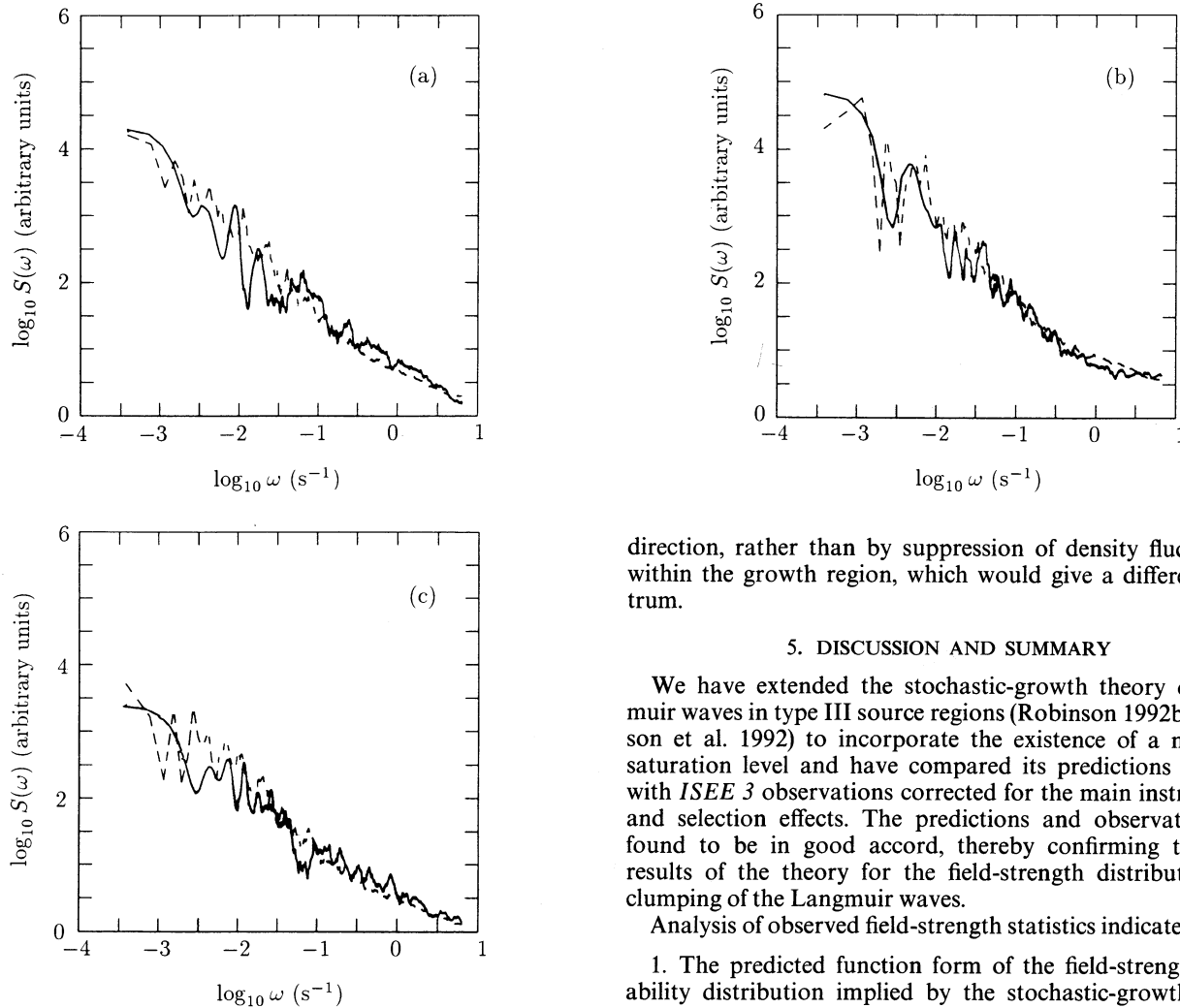
FIG. 9.—Frequency spectrum $S(\omega)$ (*solid curve*, arbitrary units) of the rolloff-corrected Langmuir fields E_A, smoothed over a range 5% either side of the nominal frequency for plotting. Dashed curve shows the corresponding Monte Carlo spectrum. (*a*) 1979 February 8 event. (*b*) 1979 February 17 event. (*c*) 1979 March 11 event.

underlying spectra corrected for instrumental effects are shown in Figures 10*a*–10*c*.

Only Celnikier et al. (1983, 1987) have independently determined the spectra of ambient density fluctuations in the solar wind for these time scales, unfortunately for two periods in which type III bursts were absent. They found spectra described by equation (19) with $a = 1.2$–1.5, $b = 2.05$–2.7, and $\omega_0 = (0.4$–1.0) s^{-1}. The shapes and parameters of the spectra found here are thus consistent with the corresponding density spectra to within their uncertainties, particularly given the considerable range of values seen, the small number of events considered here and in the analyses of ambient density fluctuations, and the absence of type III events during the density measurements. The results obtained using fields corrected for filter rolloff effects thus confirm our earlier conclusions (Robinson et al. 1992): Ambient solar-wind density fluctuations persist during type III events and determine the clumping of Langmuir waves and the consequent nonuniformities in the electron beam. Moreover, regions in which growth occurs are principally determined by alignment of ∇n with the beam direction, rather than by suppression of density fluctuations within the growth region, which would give a different spectrum.

5. DISCUSSION AND SUMMARY

We have extended the stochastic-growth theory of Langmuir waves in type III source regions (Robinson 1992b; Robinson et al. 1992) to incorporate the existence of a nonlinear saturation level and have compared its predictions in detail with *ISEE 3* observations corrected for the main instrumental and selection effects. The predictions and observations are found to be in good accord, thereby confirming the main results of the theory for the field-strength distribution and clumping of the Langmuir waves.

Analysis of observed field-strength statistics indicates:

1. The predicted function form of the field-strength probability distribution implied by the stochastic-growth theory result (12) is correct.

2. The mean wave growth/damping per interaction between a Langmuir wave clump and an inhomogeneity in the electron beam is $\langle G \rangle \sim -0.1$, and the standard deviation satisfies $\sigma(\Delta G) < 1$. Many interactions are thus required to achieve significant growth or damping, and this only occurs in a small fraction of clumps, consistent with the highly impulsive nature of the waves observed. Nonetheless, the result $\sigma(\Gamma) \gg |\langle \Gamma \rangle|$ implies that growth is positive in almost half the plasma volume at any instant. Energy lost by damped waves is approximately balanced by energy gained by growing waves to yield approximate marginal stability overall.

3. A nonlinear cutoff exists at a field strength of several mV m^{-1}, apparently independent of the characteristic Langmuir field E_{pk}.

4. The estimated fields after correction for rolloff effects are necessarily higher than the raw single-channel fields. This implies that previous theoretical estimates of fundamental and harmonic electromagnetic emissivities based on raw fields must be revised upward and that higher energy densities than previously thought are available to drive other nonlinear processes such as wave collapse.

Remaining open questions regarding the field strengths include determining the form of the probability distribution at low E_A and using a higher sampling rate to resolve short-scale
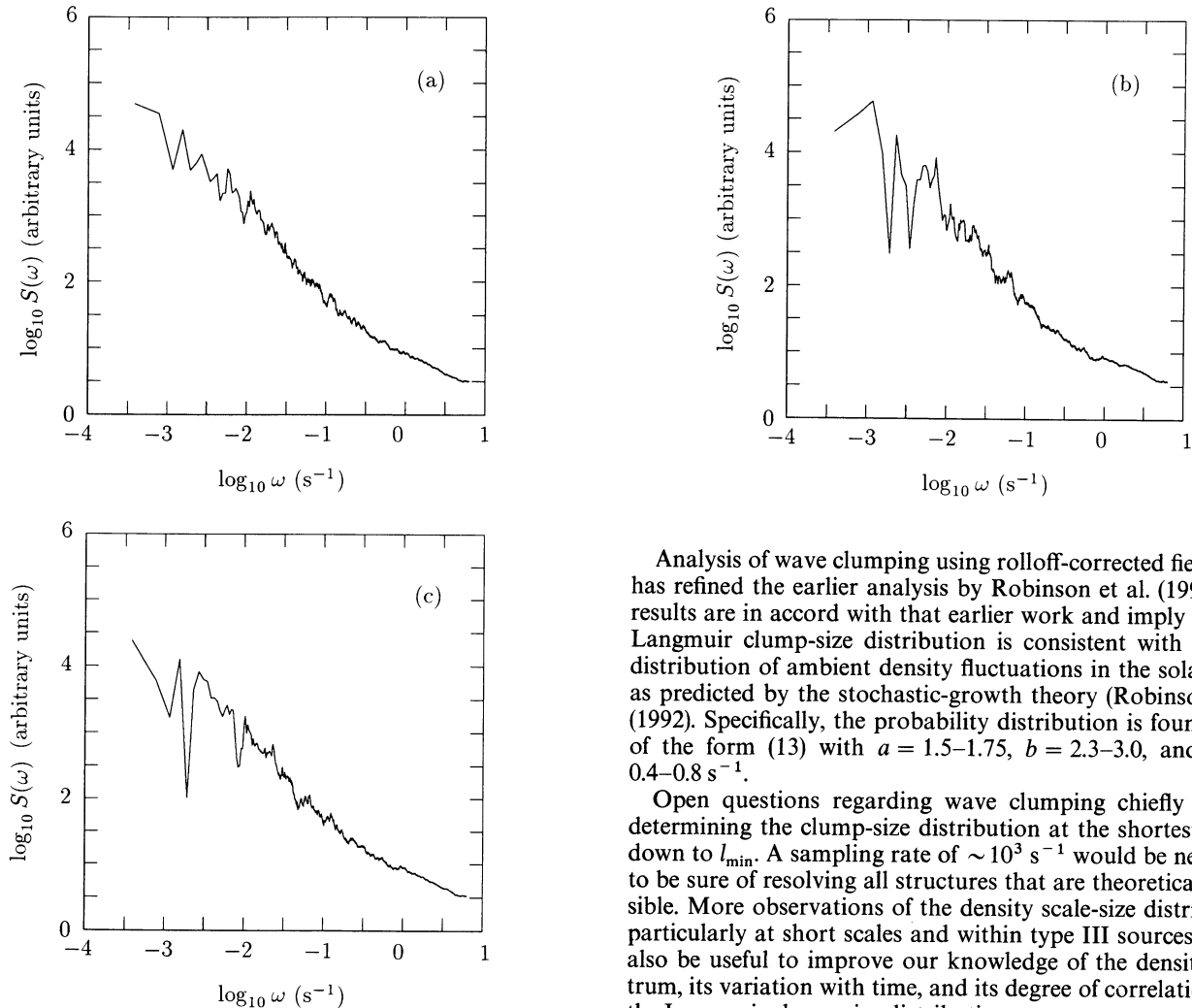
ROBINSON, CAIRNS, & GURNETT

FIG. 10.—Monte Carlo frequency spectrum $S(\omega)$ (arbitrary units) corrected for instrumental thresholds and smoothed over a range 5% either side of the nominal frequency for plotting. (a) 1979 February 8 event. (b) 1979 February 17 event. (c) 1979 March 11 event.

wave clumps. In addition, further generalization of stochastic-growth theory to incorporate the dynamics of nonlinear processes is necessary to determine the saturation mechanism responsible for the nonlinear cutoff mentioned in point 3 above and to calculate fundamental and harmonic emissivities. It is also of interest to determine why the magnitudes of $\sigma(\Gamma)$ and $\langle\Gamma\rangle$ have the observed values and whether these values are typical of weaker type III events than those considered here.

Analysis of wave clumping using rolloff-corrected fields here has refined the earlier analysis by Robinson et al. (1992). The results are in accord with that earlier work and imply that the Langmuir clump-size distribution is consistent with the size distribution of ambient density fluctuations in the solar wind, as predicted by the stochastic-growth theory (Robinson et al. (1992). Specifically, the probability distribution is found to be of the form (13) with $a = 1.5$–1.75, $b = 2.3$–3.0, and $\omega_0 = 0.4$–0.8 s^{-1}.

Open questions regarding wave clumping chiefly involve determining the clump-size distribution at the shortest scales, down to l_{min}. A sampling rate of $\sim 10^3$ s^{-1} would be necessary to be sure of resolving all structures that are theoretically possible. More observations of the density scale-size distribution, particularly at short scales and within type III sources, would also be useful to improve our knowledge of the density spectrum, its variation with time, and its degree of correlation with the Langmuir clump-size distribution.

REFERENCES

Cairns, I. H. 1984, in Proc. Course and Workshop on Plasma Astrophysics, Plasma Astrophysics (Varenna), ESA SP-207, 281
———. 1986, Ph.D. thesis, University of Sydney
Celnikier, L. M., Harvey, C. C., Jegou, R., Kemp, M., & Moricet, P. 1983, A&A, 126, 293
Celnikier, L. M., Muschietti, L., & Goldman, M. V. 1987, A&A, 181, 138
Ginzburg, V. L., & Zheleznyakov, V. V. 1958, Soviet Astron.—AJ, 2, 653
Grognard, R. J.-M. 1985, in Solar Radiophysics, ed. D. J. McLean & N. R. Labrum (Cambridge Univ. Press), 253
Gurnett, D. A., & Anderson, R. R. 1976, Science, 194, 1159
———. 1977, J. Geophys. Res., 82, 632
Lin, R. P., Levedahl, W. K., Lotko, W., Gurnett, D. A., & Scarf, F. L. 1986, ApJ, 308, 954
Lin, R. P., Potter, D. W., Gurnett, D. A., & Scarf, F. L. 1981, ApJ, 251, 364

Melrose, D. B. 1990, Sol. Phys., 130, 3
Melrose, D. B., & Cramer, N. F. 1989, Sol. Phys., 123, 343
Melrose, D. B., Dulk, G. A., & Cairns, I. H. 1986, A&A, 163, 229
Melrose, D. B., & Goldman, M. V. 1987, Solar Phys., 107, 329
Muschietti, L. 1990, Solar Phys., 130, 201
Muschietti, L., Goldman, M. V., & Newman, D. L. 1985, Sol. Phys., 96, 181
Robinson, P. A. 1992a, Sol. Phys., 137, 307
———. 1992b, Sol. Phys., 139, 147
———. 1992c, Phys. Fluids B, 4, 3524
Robinson, P. A., Cairns, I. H., & Gurnett, D. A. 1992, ApJ, 387, L101
Robinson, P. A., Willes, A. J., & Cairns, I. H. 1993, ApJ, in press
Scarf, F. L., Fredricks, R. W., Gurnett, D. A., & Smith, E. J. 1978, IEEE Trans. Geoscience Electron., GE-16, 191
Smith, D. F., & Sime, D. 1979, ApJ, 233, 998